Dendrimer-targeted immunosuppression of microglia reactivity super-accelerates photoreceptor regeneration in the zebrafish retina

Kevin B. Emmerich[1,2]*, David T. White[2]*, Siva P. Kambhamptati[2,3]*, Grace Y. Lee[2], Tian-Ming Fu[4], Arpan Sahoo[2], Meera T. Saxena[2], Eric Betzig[4#], Rangaramanujam M. Kannan[2,3#], Jeff S. Mumm[1,2,3,5#]

* Co-first author
#Corresponding authors: jmumm3@jhmi.edu, krangar1@jhmi.edu, betzige@janelia.hhmi.org

1. McKusick-Nathans Institute of the Department of Genetic Medicine, Johns Hopkins University School of Medicine, Baltimore, MD, USA
2. Department of Ophthalmology, Wilmer Eye Institute, Johns Hopkins University, Baltimore, MD, USA
3. The Center for Nanomedicine, Wilmer Eye Institute, Johns Hopkins University, Baltimore, MD, USA
4. Janelia Farms Research Campus, Howard Hughes Medical Institute, Ashburn, VA, USA
5. Department of Neuroscience, Johns Hopkins University, MD, USA

Abstract

Retinal regeneration occurs naturally in zebrafish but not in mammals. A thorough understanding of the mechanisms regulating regeneration may help to advance strategies for stimulating retinal repair in humans. We previously implicated microglia as key regulators of retinal regeneration using a zebrafish model of inducible photoreceptor degeneration. Intriguingly, post-injury treatments with the immune suppressant dexamethasone (Dex) resulted in accelerated photoreceptor regeneration. Modifying microglia responses to retinal cell death may therefore promote neuroregenerative processes. Here, we investigated the effect of Dex on microglia reactivity in the regenerating zebrafish retina using adaptive optics-corrected lattice light-sheet microscopy. Quantitative analysis of *in vivo* time-lapse imaging data revealed that Dex inhibited microglia migration speed, consistent with an immunosuppressive effect. Unfortunately, long-term treatment with glucocorticoids, including Dex, causes adverse side effects which limits their use therapeutically. To overcome this limitation, a nanoparticle-based drug delivery strategy was used to target Dex to reactive microglia. We show that conjugating Dex to dendrimer nanoparticles: 1) dramatically decreased toxicity in larval zebrafish, 2) succeeded in selective targeting of reactive microglia and, 3) resulted in "super-accelerated" photoreceptor regeneration kinetics. These data support the use of dendrimer-based drug formulations for modulating microglia reactivity in degenerative disease contexts, especially as therapeutic strategies for promoting regenerative responses to neuronal cell loss.

Keywords: Photoreceptor, Regeneration, Dendrimer, Nitroreductase, Microglia

Introduction

Neurodegenerative diseases are caused by the loss of specific neuronal cell types. In humans, this loss is permanent because adult mammals do not regenerate central nervous system (CNS) neurons. In contrast, teleost fish and particularly zebrafish exhibit a robust capacity for regeneration (1–4) Therapies aimed at promoting dormant neuronal regenerative capacities could provide a means of reversing neurodegenerative disease to promote recovery of neural function. However, developing neuroregenerative therapeutics is complicated by the need for compounds to cross the blood-brain barrier (BBB) and/or blood-retinal barrier (BRB) (5). Additionally, therapeutic compounds must have minimal off-target effects. Due to these requirements, compounds shown to be effective *in vitro* or *in silico* often fail or have reduced efficacy in animal models and/or clinical trials.

Nanomedicine-based innovations can be used to promote transport across the BBB/BRB permeability, improve targeting, and achieve sustained delivery to increase drug efficacy. Dendrimer nanoparticles, for instance, have been shown to improve delivery to the CNS (6). Dendrimers are well-defined tree-like molecules synthesized to allow for precise size, charge, and molecular weight (7–9). They can also be conjugated to multiple cargo (e.g., drug), or types of cargo (e.g., drug and reporter), per molecule. This tunable nature allows selection for qualities that work best for specific applications. For instance, hydroxyl dendrimers ~3-6nm in size can cross the impaired BBB/BRB efficiently, and localize specifically to reactive microglia and macrophages, and can reduce drug toxicity compared to free drug regimens (9–11).

The majority of studies on neuroimmune interactions during neurodegeneration have focused on ameliorating negative consequences of chronic inflammation. However, prior studies using zebrafish—a naturally regenerative species—indicate the immune system can beneficially contribute to neuronal regeneration (12, 13). Intriguingly, the immune system has been shown to regulate neuronal regenerative capacities in mammals as well (14). We previously implicated microglia as key regulators of rod photoreceptor regeneration in the zebrafish retina. In addition, we found differential effects of immune reactivity over the course of regeneration. Consistent with prior studies, suppressing immune reactivity with dexamethasone (Dex) prior to neuronal cell loss disrupted the regenerative process. Uniquely, when immune suppression was delayed until the day after initiation of neuronal cell loss, the regenerative process was accelerated (15). These results imply that immune system reactivity initially promotes, but subsequently suppresses neuronal regeneration in zebrafish. However, as Dex has significant systemic effects, attributing Dex-associated findings solely to immunosuppression is problematic. Targeted delivery of Dex to reactive immune cells would provide a means of addressing this limitation, and help elucidate the specific role of reactive microglia.

In addition to reducing side-effects, dendrimer-based drug delivery enables selective cell targeting. One example of this includes hydroxyl (poly)amidoamine (PAMAM) dendrimers that target reactive immune cells (16, 17), without the need for targeting ligands. Dendrimer conjugation to Dexamethasone (D-Dex), a glucocorticoid and immune suppression drug, was shown to target activated macrophages in a rabbit model for autoimmune dacryoadenitis and ultimately led to improved clinical phenotypes. Additionally, D-Dex was used to attenuate inflammation by targeting macrophages in a model of corneal alkali burn (18). We have previously shown that systemic or local hydroxyl dendrimers and dendrimer-drug conjugates target reactive microglia/macrophages in multiple small and large animal models of CNS and ocular disorders (19–22). One caveat of prior studies arises from the use of static imaging to assess dendrimer-based microglia/macrophage targeting. Here, *in vivo* time-lapse imaging will be used to further evaluate the dynamics of dendrimer-based targeting of reactive immune cells. While it is clear that dendrimer-drug conjugates are able to quell neuroinflammation following injury, which has also been shown in neuronal degeneration (17), they have yet to be tested for effects on neuronal regeneration. We were therefore interested in investigating if dendrimer conjugation can enhance the regeneration-promoting effects of Dex we previously observed.

Here, using an inducible zebrafish model of retinitis pigmentosa (RP), we investigated the effects of post-injury Dex treatment on microglia reactivity in the retina. Adaptive optical lattice light-sheet microscopy (AO-LLSM) (23), was used to follow microglia dynamics at high spatial and temporal resolution *in vivo*. Next, we compared the effects of free Dex to dendrimer-conjugated Dex (D-Dex) on retinal regeneration kinetics. Results confirm past findings regarding the immune suppressing effects of post-injury Dex treatments and show that D-Dex improves the beneficial effects of post-injury immune suppression on neuronal regeneration: reducing toxicity, promoting selective targeting of reactive immune cells, and greatly enhancing the regeneration-promoting effects of Dex-based immunosuppression.

Results

Post-ablation Dex treatment reduces microglia speed

Our initial characterization of the effects of immune suppression on retinal regeneration indicated that Dex could either inhibit or promote rod photoreceptor replacement depending on the timing of treatment. Pre-treating with Dex, prior to induction of rod cell ablation, inhibited regeneration. However, when Dex was applied a day after rod cell loss had been initiated, rod cell regeneration kinetics accelerated (15). Mechanistically, *in vivo* imaging showed that pre-treating with Dex inhibited microglia reactivity to rod cell death. However, the mechanistic effects of treating with Dex post-injury, the paradigm that enhanced regeneration, remain unknown. To address this question, we utilized a powerful new intravital imaging technique developed by the Betzig lab, AO-LLSM (23–25), to follow microglia dynamics at high spatial and temporal resolution *in vivo* with or without Dex treatment after induction of rod cell death.

For AO-LLSM imaging, a transgenic line that labels and enables selective ablation of rod photoreceptors (i.e., expressing a YFP-NTR fusion protein) was crossed with a transgenic line labeling macrophages and microglia with a complementary fluorescent reporter (e.g., CFP or Cherry). Dual-labeled transgenic larvae were selected and treated with the prodrug metronidazole (MTZ) at 5 days post-fertilization (dpf) to induce ablation of YFP-NTR expressing rod photoreceptor cells (non-ablated larvae served as controls). After 24 h, MTZ was removed and larvae in each group, ablated and non-ablated, were treated with 2.5 μM Dex (to accelerate regeneration kinetics) or control media. AO-LLSM-based high resolution intravital imaging was used to monitor interactions between microglia and rod cells in all four treatment groups starting at 5.5 dpf (e.g., 12 hrs post-MTZ treatment). Labeled cells were 3D-rendered in Imaris and migration speeds and sphericity of microglia (and peripheral macrophages) were quantified as metrics of reactivity. Microglia in non-ablated control fish, treated with or without Dex, exhibited ramified morphologies, actively extending and retracting cellular processes, but remained relatively non-migratory, consistent with a non-reactive, homeostatic state (Fig. 1A, B, Supp Videos 1 and 2). Conversely, microglia in the ablated groups had largely spheroid morphologies suggestive of reactivity. Microglia in MTZ-treated larvae that were not treated with Dex became highly motile, rapidly migrating in and among the dying rod cells (Fig. 1C, Supp Video 3). Despite retaining amoeboid morphologies, microglia in ablated larvae treated with Dex remained static (Fig. 1D, Supp Video 4). Quantitative analysis of 3D morphologies confirmed the transition from ramified to amoeboid profiles among microglia in ablated larvae (Fig. 1E). In addition, quantification of migration speed showed microglia in ablated larvae not treated with Dex were more motile than the other three groups, averaging 9.68 microns per second. No statistically significant differences in migratory behavior were observed between the non-ablated controls ±Dex and/or ablated larvae treated with Dex (Fig. 1F).

Dendrimer-conjugated dexamethasone (D-Dex) is non-toxic compared to free Dex

Long-term therapeutic use of Dex and other glucocorticoids is complicated by multiple adverse side-effects and systemic toxicity concerns (26). Therefore, we were interested in exploring options for reducing the deleterious effects of Dex, as well as isolating the effect of Dex on microglia rather than systemically. Based on previous studies which utilized dendrimer-drug nanoparticles to target reactive microglia and reduce drug toxicity (9, 10, 20, 21, 27), we conjugated a generation 4 (G4-OH) PAMAM dendrimer to Dex (D-Dex). The D-Dex conjugates used in this study were >98% pure and has ~8 molecules of Dex conjugated to the surface

hydroxyl groups of the PAMAM dendrimers as reported previously (10, 18). To test toxicity, the pericardium of living zebrafish larvae were injected with Dex, D-Dex or vehicle alone at 5 days-post fertilization (dpf); at Dex concentrations that ranged from 2.5-400 μM (Fig. 2A). Mortality rates for each condition were measured two days following treatment (7 dpf).

At lower concentrations, 2.5 - 25 μM, no death was observed amongst the three injection groups (Dex, D-Dex or vehicle). However, free Dex treated fish had increased mortality rates at higher concentrations, demonstrating up to 75% toxicity at 400 μM. In stark contrast, only ~5% of fish treated with 400 μM D-Dex died while no vehicle injected fish died. The LD50 of unconjugated Dex, the concentration that results in the death of half of the treated population, was between 200 - 400 μM (Fig. 2B). These findings are in agreement with previous studies in which D-Dex attenuated Dex toxicity ~10-fold (18).

D-Dex post-ablation treatment super-accelerates rod photoreceptor regeneration

We previously observed a 30% increase in rod PR regeneration kinetics when fish were treated with free Dex 24 hours following ablation with MTZ, compared to MTZ only treated controls (15). Here, we used the same fluorescent plate reader assay (28) to test compare the effects of Dex and D-Dex injection on rod cell regeneration kinetics in zebrafish larvae (Fig. 3A). YFP-NTR expressing transgenic larvae were first exposed to 10 mM MTZ for 24 hr from 5-6 dpf to induce rod cell ablation; loss of YFP-expressing rod cells was visually confirmed using stereo-fluorescence microscopy. MTZ as then removed and larvae were subjected to pericardial injection of free Dex or D-Dex; MTZ-exposed larvae soaked in free Dex or vehicle alone served as controls. At 9 dpf, 72h into the regenerative phase, rod cell regeneration kinetics (i.e. the return of the YFP signal) was measured using a fluorescent plate reader (Fig. 3A). Compared to control MTZ-exposed larvae, all three Dex treated conditions resulted in enhanced rod PR regeneration kinetics. However, statistically significant increases were only observed for larvae soaked in free Dex or injected with D-Dex. The increase in regeneration kinetics observed with free Dex, ~30%, was on par with our previous findings (15). Intriguingly, larvae injected with D-Dex showed a ~67% enhancement in rod PR regeneration kinetics compared to control MTZ treated fish; 51% more than free Dex injections and nearly double the rate of larvae soaked in free Dex (Fig. 3B).

D-Dex localizes to dying rod photoreceptors and subsequently to reactive phagocytes

We next sought to determine whether D-Dex works locally at the site of injury or systemically by visualizing where dendrimers accumulate post-injection. Previous data from static images suggest dendrimer nanoparticles accumulate in reactive microglia/macrophages at sites of injury/inflammation (10). Here, we evaluated dendrimer localization *in vivo* dynamically using intravital time series confocal imaging (Fig. 4A, B). To monitor interactions between dendrimers and retinal microglia following rod cell ablation we used double transgenic fish expressing NTR-YFP in rods and RFP in microglia. To promote a more sustained inflammatory environment, we prolonged the cell ablation process by treating larvae with a decreased concentration of MTZ (2.5 mM) for 48 hr, from 5-7 dpf. Midway through this process, at 6 dpf, D-Cy5 was pericardially injected and time-series confocal microscopy used to assess D-Cy5 localization in the retina. At 90 min post-injection, D-Cy5 co-localized with dying rod cells in the outer nuclear layer (ONL; Fig. 4C, inset). Although presumably reactive microglia were observed nearby, no evidence of co-localization with D-Cy5 was observed at this time. In contract, by 270 min post-

injection, RFP-expressing retinal microglia and peripheral macrophages co-localized strongly with D-Cy5 (Fig. 4D). To better monitor dynamic interactions between D-Cy5 and labeled cells, confocal timelapse imaging was used as per our prior report (15). In a 4D-rendered video in which imaging begins 30 hrs post-MTZ treatment and 6 hrs post-injection of D-Cy5, frequent examples of microglia acquiring D-Cy5 are observed following initial D-Cy5 localization near dying rod PRs (Supp Video. 5).

Finally, we were interested in quantifying targeting and preferential uptake of dendrimer D-Cy5 to microglia/macrophages and rod PRs based on measurable cell features including sphericity, area, and volume. Upon activation, reactive microglia undergo a morphology change that is broadly marked by a more spherical shape (29). Using morphometric analysis we previously implemented (15), we rendered and colorized rod PRs and microglia/macrophages relative to the intensity of D-Cy5 at 90- and 270-minutes post injection into the pericardium.

Observationally, it appeared that retinal microglia proximal to D-Cy5+ rod PRs took up D-Cy5 faster than other areas of the retina (Supp Fig. 6 A-A', B-B'). In attempts to quantify this, we used IMARIS software to measure sphericity, volume, and surface area of PRs and microglia/macrophages relative to D-Cy5 intensity. This analysis showed no strong correlations between any of these three parameters with D-Cy5 intensity (Supp Fig 1. C-C', D-D').

Discussion

Highly dynamic interactions between the immune and nervous systems—i.e., the neuroimmune system—play important beneficial roles during neurodevelopment, in maintaining synaptic homeostasis, and in regulating adult neurogenesis (30–32). During neurodegenerative disease, neuroimmune activity is context-dependent, changing relative to acute versus chronic inflammatory states. Neuroimmune interactions generally exacerbate chronic neurodegenerative processes (33, 34). However, roles during acute neuroinflammation, appropriate modulation of neuroimmune interactions can be beneficial (35, 36). That microglia/macrophages appear to play beneficial roles during neuronal regeneration in zebrafish supports the hypothesis that the immune system can positively impact neural repair (15, 37).

Our lab developed a targeted cell-ablation system that enables prodrug-induced cell death in multiple disease-relevant cell types. We previously observed that induction rod cell death, is followed by hallmarks of retinal microglial activation including migration toward dying rod cells and subsequent local proliferation. Treatment with immune suppressant Dex either increased and decreased rod cell regeneration kinetics depending on the time of treatment relative to MTZ-induced rod cell ablation. When Dex treatment followed rod cell death, regeneration kinetics were accelerated by ~30% (15). We posit this is due to Dex suppression of anti-reparative microglia reactivity, consistent with inhibit neuronal regeneration in the CNS (38). Here, we build upon these findings by incorporating AO-LLSM imaging of microglia responses to rod cell death and utilizing PAMAM dendrimers to deliver Dex directly to reactive microglia. The former improves spatiotemporal resolution of neuroimmune interactions during rod cell death. The latter tests the effects of targeted immunosuppression on rod cell regeneration kinetics.

Previous intravital imaging assays revealed the pre-ablation Dex treatments eliminated microglia reactivity to rod cell death, in turn inhibiting regeneration (15). Here, AO-LLSM was used to

monitor the effects of post-ablation Dex treatments on microglia behavior. Dex significantly decreased microglia migration speed but did not alter microglia morphology (i.e., sphericity). This was surprising, as sphericity has long been tied to microglia/macrophage reactivity, thus Dex was anticipated to decrease sphericity. It is unclear how a reduction in migration speed alone results in enhanced regeneration kinetics. Thus our data supports the idea that post-ablation Dex treatments suppress pro-inflammatory and/or anti-reparative microglia reactivity to promote regeneration, despite the lack of near-term effects on sphericity. Interestingly, the proposed anti-reparative phase follows an initial pro-regenerative phase—per our prior results showing pre-Dex treatments abolish the regenerative process—consistent with dynamically opposing functions of microglia (36) or possibly microglia subtypes (39, 40). These results contrast somewhat with presumed roles for "M1" and "M2" microglia in that the initial response would be presumed to be reactive, thus anti-reparative, and the latter phase would be expected to be pro-reparative. A recent transcriptomic profiling of zebrafish microglia in the regenerating retina focused on a later phase of the regenerative process (41) showed upregulation of factors promoting phagocytic activity consistent with sustained reactivity and highlighting the need for comparisons to earlier time points corresponding to the peak of cell death. Importantly, the increased spatiotemporal resolution provided by AO-LLSM imaging revealed that peripheral macrophages do enter the retina following MTZ-induced rod cell ablation (Supp Fig. 2), in contrast to our prior observations using much slower scanning confocal microscopy. Thus, alternatively, post-ablation Dex could function to inhibit anti-reparative effects of infiltrating macrophages

PAMAM dendrimers provide a unique opportunity to selectively target reactive immune cell types, affording new opportunities to assess immune cell dynamics and function. Therefore, dendrimer conjugation of drugs enables us to gain insights specifically on the role of reactive microglia and macrophages on the regenerative process. In addition, conjugating drugs to dendrimers has been found to be comparatively less toxic to cells and living organisms than comparable free drug treatments, presumably due to rapid kidney clearance in the absence of inflammation (16). As Dex can cause significant deleterious effects, dendrimer-based reductions in toxicity are particularly relevant. Thus, we conjugated Dex to G4 PAMAM dendrimers (D-Dex) and tested D-Dex for reduced toxicity, neuronal regeneration kinetics, and immune cell targeting. Pericardial injection of D-Dex was performed to enable effective delivery to the retina as done in other studies with D-Dex (18). The data showed that pericardially injected D-Dex: 1) is substantially less toxic than injected free Dex, 2) super-accelerated rod cell regeneration kinetics (~67% increase) ~relative to soaking in or injection of free Dex (~34% and ~51% increases, respectively), and 3) targeted both dying rod cells and reactive microglia/macrophages. The temporal dynamics of the latter result suggested that dendrimers target dying neurons first and secondarily accumulate in phagocytic microglia/macrophages. Each of these findings is novel and builds upon an expanding body of work demonstrating profound therapeutic potential of dendrimer nanoparticles (7, 17, 27).

In summary, we report here the use of dendrimer nanoparticles in zebrafish to promote neuronal regeneration via targeted delivery of an immunosuppressant to reactive immune cells. Collectively, our data are consistent with microglia and/or macrophages transitioning to an anti-regenerative profile after an initial pro-regenerative response. Novel findings include imaging data suggesting that dendrimers target dying neurons and subsequently accumulate in phagocytic

immune cells and the capacity of D-Dex injections to super-accelerate neuronal regeneration kinetics. The latter finding has broad therapeutic potential and underscores the need to further our understanding of the role of the neuroimmune system in neurodegenerative and neuroregenerative processes.

Materials and Methods

Zebrafish husbandry and transgenic lines

All studies were carried out in accordance with recommendations of OLAW for zebrafish studies and an approved Johns Hopkins University Animal Care and Use Committee animal protocol FI17M19. All fish were maintained using established conditions at 28.5◦C with a consistent 14:10 h light:dark cycle. Transgenic lines used include Tg(rho:YFP Eco. NfsB)gmc500 (rho:YFP-NTR) and Tg(mpeg1:GAL4-VP16) which have been previously published (15, 28, 42–46). Tg(rho:YFP Eco. NfsB)gmc500 expresses a bacterial Nitroreductase (NTR) enzyme selectively in rod PRs to enable selective ablation (see below). This line was further propagated in a pigmentation mutant, roy^{a9} (roy), to facilitate detection of YFP signal *in vivo*.

NTR-MTZ mediated rod photoreceptor ablation and free-Dex treatment

NTR:YFP expressing larvae were separated into equal-sized groups at 5 dpf: (i) nontreated controls and (ii) larvae treated with either 10 mM Metronidazole (MTZ, Acros) for 24 hr or 2.5 mM MTZ for 48 hr at 5 dpf (specifically to slow down the injury process for *in vivo* confocal imaging). MTZ is reduced by NTR into a cytotoxic substance inducing DNA-damage followed by specific cell death. After MTZ treatment, fish were rinsed and kept in 0.3Å~ Danieau's solution until quantified, imaged or killed.
For experiments with non-conjugated Dex treatment, equal size groups of fish ablated with MTZ were treated with 2.5 μM Free-Dex. Fish treated with Dex only as controls were additionally used as well as untreated fish.

Adaptive optics lattice light-sheet microscopy (AO-LLSM)

5-7 dpf zebrafish were anesthetized using tricaine (0.16 mg/ml) and then embedded in a 0.8% low melt agarose droplet on a 25-mm coverslip. A homemade hair-loop was used to position and orient fish. The excitation and detection objectives along with the 25-mm coverslip were immersed in ~40 ml of E3 media + PTU at room temperature (22 ± 1° C). Zebrafish expressing *Tg(rho:YFP Eco. NfsB)gmc500* ("rho:YFP-NTR") and *Tg(mpeg1:TdTomato)*—to label rod photoreceptors and microglia/macrophages, respectively (15)—were excited using 514 nm and 560 nm lasers simultaneously (514 nm operating at ~3 mW and 560 nm operating at 5 mW corresponding to ~15 μW and ~25 μW at the back aperture of the excitation objective) with an exposure time of 20-50 msec. Dithering lattice light-sheet patterns with an inner/outer numerical aperture of 0.36/0.4 for both colors were used. The optical sections were collected by scanning the sample stage with 400-500 nm step size, equivalent to 200-250 nm axial step size in detection objective coordinate, with a total of 121-201 steps. Emission light from the two fluorophores were separated by a long-pass filter (Di03-R561-t3, Semrock, USA) and captured by two Hamamatsu ORCA-Flash 4.0 sCMOS cameras (Hamamatsu Photonics, Hamamatsu City, Japan). Prior to the acquisition of the time series data consisting of 100–200 time points, the imaged volume was corrected for optical aberrations using two-photon "guide star" based adaptive optics method (manuscript in preparation). Each imaged volume was deskewed and deconvolved with experimentally measured point spread functions obtained from 100 nm

tetraspec beads (Thermo Fisher) in C++ using Richardson-Lucy algorithm on HHMI Janelia Research Campus' computing cluster. The AO-LLSM was operated using a custom LabVIEW software (National Instruments, Woburn, MA). Image analysis was performed using FiJi (i.e., ImageJ v1.52p; NIH) or Imaris (v9.5.1; Bitplane) to quantify by analysis including displacement and speed of microglia.

Synthesis of fluorescently labeled dendrimer (D-Cy5) and dendrimer-dexamethasone (D-Dex) conjugates

To enable imaging of dendrimer in this zebrafish model, we fluorescently labeled the hydroxyl terminated generation 4 PAMAM dendrimers (G4-OH) by covalently conjugating a near IR dye Cyanine 5 (Cy5) to the surface -OH groups of the dendrimers to obtain D-Cy5. These protocols have been previously published (47, 48). The D-Cy5 conjugate was characterized for its loading and purity using proton-nuclear magnetic resonance (^{1}H NMR) and high-performance liquid chromatography (HPLC) respectively. Dendrimer-dexamethasone conjugate (D-Dex) was synthesized by following previously reported synthesis procedure (18). Briefly, the D-Dex conjugates were synthesized using a two-step procedure. In the first step, dexamethasone-21-glutarate (Dex-linker) was synthesized by reacting the -OH group at the 21st position of Dex to the -COOH of the glutaric acid in the presence of triethylamine as a base. The Dex-Linker was purified using flash column chromatography. In the second step, the Dex-Linker was conjugated to the -OH groups on the dendrimer surface in the presence of coupling agent benzotriazol-1-yloxy tripyrrolidinophosphonium hexafluorophosphate diisopropylethylamine (PyBOP) as a base and anhydrous dimethylformamide (DMF) as solvent. The final product was purified using dialysis against DMF to remove reacted Dex-linker and PyBOP side products for 24 hours followed by dialysis against water to remove DMF. D-Dex conjugate was characterized using ^{1}H NMR to estimate the drug loading and HLPC for its purity.

Intravital confocal microscopy

All intravital imaging applied previously detailed protocols (49–51). Confocal z-stacks encompassing the entire orbit of the eye (step size, 5 microns) were collected at 10- or 20-min intervals over a total of between 4.5 and 20 hours. Image analysis was performed using FiJi (i.e., ImageJ v1.49b; NIH) or Imaris (v7.6.5; Bitplane) to quantify by morphometric analysis as sphericity, correlation between are and volume.

IMARIS volumetric rendering and quantification.

Larval whole-retina images were collected as described above using identical acquisition and IMARIS processing parameters across all conditions. Photoreceptor volume was calculated using IMARIS local background-based volumetric rendering of YFP signals.

ARQiv scans to measure rod photoreceptor regeneration kinetics

Transgenic rho:YFP-NTR larvae were treated with MTZ ± Dex, and regeneration kinetics were analyzed using the ARQiv system, as previously described (28, 52). 5 dpf larvae were exposed to 10 mM MTZ for 24 hours and then were treated with a single dose of 2.5 μM Free-Dex or treated with D-Dex (see below). The ARQiv scan was performed on day 9.

Pericardial injection of Dex and dendrimer-conjugated Dex and D-Cy5

Transgenic rho:YFP-NTR larvae were treated with MTZ at 5 dpf, and then at 6 dpf larvae were anesthetized with Tricaine, place under a PLI-100 picospritzer (Harvard Apparatus) and injected with 10 nL amount of either 5 μM Dex, D-Dex or D-Cy5. Concentration was doubled compared to Free-Dex to account for differential uptake under injection compared to soaking. Subsequently at day 9 the ARQiv scan was performed to measure regeneration kinetics as above. In later experiments, injection was performed with D-Cy5 in order to observe Dendrimer activity in *vivo*. Toxicity of this injection method was determined following injection of equal groups of fish with vehicle, and various concentrations of Free-Dex, or D-Dex (containing equivalent Dex in conjugated form) at 5 dpf. At 7 dpf, % of surviving fish was counted (Fig 2).

Statistical analysis

Data were processed with a custom R-based package (ggplot2) to generate box plots showing the first quartile (lower box), median (bold line), third quartile (upper box), upper and lower adjacent (whiskers), and raw data (dot plot; large dots denote outlier observations) for each experimental condition. Statistical analyses were carried out with R 3.3.1 and RStudio 0.99.893. Student's t test was used to calculate effect size between paired groups with effect size, 95% confidence intervals, and P values provided.

Acknowledgements

This work was supported by the following grants from the National Institutes of Health, R01OD020376 (JSM).

Competing interests

JSM holds patents for the NTR inducible cell ablation system (US #7,514,595) and uses thereof (US #8,071,838 and US#8431768). All other authors have no commercial relationships.

References

1. Andersson O, et al. (2012) Adenosine signaling promotes regeneration of pancreatic β cells in vivo. *Cell Metab*. doi:10.1016/j.cmet.2012.04.018.
2. Choi WY, et al. (2013) In vivo monitoring of cardiomyocyte proliferation to identify chemical modifiers of heart regeneration. *Dev*. doi:10.1242/dev.088526.
3. Gorsuch R a, Hyde DR (2014) Regulation of Müller glial dependent neuronal regeneration in the damaged adult zebrafish retina. *Exp Eye Res* 123:131–40.
4. Gemberling M, Bailey TJ, Hyde DR, Poss KD (2013) The zebrafish as a model for complex tissue regeneration. *Trends Genet*. doi:10.1016/j.tig.2013.07.003.
5. Saraiva C, et al. (2016) Nanoparticle-mediated brain drug delivery: Overcoming blood-brain barrier to treat neurodegenerative diseases. *J Control Release*. doi:10.1016/j.jconrel.2016.05.044.
6. Patel T, Zhou J, Piepmeier JM, Saltzman WM (2012) Polymeric nanoparticles for drug delivery to the central nervous system. *Adv Drug Deliv Rev*. doi:10.1016/j.addr.2011.12.006.
7. Kannan RM, Nance E, Kannan S, Tomalia DA (2014) Emerging concepts in dendrimer-based nanomedicine: From design principles to clinical applications. *J Intern Med*. doi:10.1111/joim.12280.
8. White DT, Saxena MT, Mumm JS (2019) Let's get small (and smaller): Combining

zebrafish and nanomedicine to advance neuroregenerative therapeutics. *Adv Drug Deliv Rev*. doi:10.1016/j.addr.2019.01.011.
9. Kurtoglu YE, Mishra MK, Kannan S, Kannan RM (2010) Drug release characteristics of PAMAM dendrimer-drug conjugates with different linkers. *Int J Pharm*. doi:10.1016/j.ijpharm.2009.10.017.
10. Lin H, et al. (2018) Subconjunctival dendrimer-drug therapy for the treatment of dry eye in a rabbit model of induced autoimmune dacryoadenitis. *Ocul Surf*. doi:10.1016/j.jtos.2018.05.004.
11. del Amo EM, et al. (2017) Pharmacokinetic aspects of retinal drug delivery. *Prog Retin Eye Res*. doi:10.1016/j.preteyeres.2016.12.001.
12. Var SR, Byrd-Jacobs CA (2019) Microglial response patterns following damage to the zebrafish olfactory bulb. *IBRO Reports*. doi:10.1016/j.ibror.2019.08.002.
13. Bosak V, Murata K, Bludau O, Brand M (2018) Role of the immune response in initiating central nervous system regeneration in vertebrates: Learning from the fish. *Int J Dev Biol*. doi:10.1387/ijdb.180033vb.
14. Baldwin KT, Carbajal KS, Segal BM, Giger RJ (2015) Neuroinflammation triggered by β-glucan/dectin-1 signaling enables CNS axon regeneration. *Proc Natl Acad Sci U S A*. doi:10.1073/pnas.1423221112.
15. White DT, et al. (2017) Immunomodulation-accelerated neuronal regeneration following selective rod photoreceptor cell ablation in the zebrafish retina. *Proc Natl Acad Sci U S A*. doi:10.1073/pnas.1617721114.
16. Sharma A, et al. (2018) Targeting mitochondrial dysfunction and oxidative stress in activated microglia using dendrimer-based therapeutics. *Theranostics*. doi:10.7150/thno.29039.
17. Iezzi R, et al. (2012) Dendrimer-based targeted intravitreal therapy for sustained attenuation of neuroinflammation in retinal degeneration. *Biomaterials*. doi:10.1016/j.biomaterials.2011.10.010.
18. Soiberman U, et al. (2017) Subconjunctival injectable dendrimer-dexamethasone gel for the treatment of corneal inflammation. *Biomaterials*. doi:10.1016/j.biomaterials.2017.02.016.
19. Kannan S, et al. (2012) Dendrimer-based postnatal therapy for neuroinflammation and cerebral palsy in a rabbit model. *Sci Transl Med*. doi:10.1126/scitranslmed.3003162.
20. Nance E, et al. (2016) Nanoscale effects in dendrimer-mediated targeting of neuroinflammation. *Biomaterials*. doi:10.1016/j.biomaterials.2016.05.044.
21. Nance E, et al. (2017) Dendrimer-mediated delivery of N-acetyl cysteine to microglia in a mouse model of Rett syndrome. *J Neuroinflammation*. doi:10.1186/s12974-017-1004-5.
22. Grimm JC, et al. (2016) Nanotechnology Approaches to Targeting Inflammation and Excitotoxicity in a Canine Model of Hypothermic Circulatory Arrest–Induced Brain Injury. *Annals of Thoracic Surgery* doi:10.1016/j.athoracsur.2016.02.077.
23. Liu TL, et al. (2018) Observing the cell in its native state: Imaging subcellular dynamics in multicellular organisms. *Science (80-)*. doi:10.1126/science.aaq1392.
24. Wang K, et al. (2014) Rapid adaptive optical recovery of optimal resolution over large volumes. *Nat Methods*. doi:10.1038/nmeth.2925.
25. Chen BC, et al. (2014) Lattice light-sheet microscopy: Imaging molecules to embryos at high spatiotemporal resolution. *Science (80-)*. doi:10.1126/science.1257998.
26. Riffo-Vasquez Y, Venkatasamy R, Page CP (2018) Steroid sparing effects of doxofylline.

Pulm Pharmacol Ther. doi:10.1016/j.pupt.2017.10.008.
27. Sharma R, et al. (2017) Activated Microglia Targeting Dendrimer-Minocycline Conjugate as Therapeutics for Neuroinflammation. *Bioconjug Chem*. doi:10.1021/acs.bioconjchem.7b00569.
28. Walker SL, et al. (2012) Automated reporter quantification in vivo: High-throughput screening method for reporter-based assays in zebrafish. *PLoS One* 7(1):e29916.
29. Davis EJ, Foster TD, Thomas WE (1994) Cellular forms and functions of brain microglia. *Brain Res Bull*. doi:10.1016/0361-9230(94)90189-9.
30. Bessis A, Béchade C, Bernard D, Roumier A (2007) Microglial control of neuronal death and synaptic properties. *Glia*. doi:10.1002/glia.20459.
31. Schafer DP, et al. (2012) Microglia Sculpt Postnatal Neural Circuits in an Activity and Complement-Dependent Manner. *Neuron*. doi:10.1016/j.neuron.2012.03.026.
32. Walton NM, et al. (2006) Microglia instruct subventricular zone neurogenesis. *Glia*. doi:10.1002/glia.20419.
33. Karlstetter M, et al. (2015) Retinal microglia: Just bystander or target for therapy? *Prog Retin Eye Res*. doi:10.1016/j.preteyeres.2014.11.004.
34. Richard M. Ransohoff (2016) How neuroinflammation contributes to neurodegeneration. *Science (80-)*. doi:10.1126/science.aag3194.
35. Plaza-Zabala A, Sierra-Torre V, Sierra A (2017) Autophagy and microglia: Novel partners in neurodegeneration and aging. *Int J Mol Sci*. doi:10.3390/ijms18030598.
36. Cherry JD, Olschowka JA, O'Banion MK (2014) Neuroinflammation and M2 microglia: The good, the bad, and the inflamed. *J Neuroinflammation*. doi:10.1186/1742-2094-11-98.
37. Thomas JL, Ranski AH, Morgan GW, Thummel R (2016) Reactive gliosis in the adult zebrafish retina. *Exp Eye Res*. doi:10.1016/j.exer.2015.09.017.
38. Hu X, et al. (2015) Microglial and macrophage polarization - New prospects for brain repair. *Nat Rev Neurol*. doi:10.1038/nrneurol.2014.207.
39. Stratoulias V, Venero JL, Tremblay M, Joseph B (2019) Microglial subtypes: diversity within the microglial community. *EMBO J* 38(17):1–18.
40. Hoang T (2019) Cross-species transcriptomic and epigenomic analysis reveals key regulators of injury response and neuronal regeneration in vertebrate retinas. *Bioarxiv*. doi:10.1017/CBO9781107415324.004.
41. Mitchell DM, Sun C, Hunter SS, New DD, Stenkamp DL (2019) Regeneration associated transcriptional signature of retinal microglia and macrophages. *Sci Rep*. doi:10.1038/s41598-019-41298-8.
42. Petrie TA, Strand NS, Tsung-Yang C, Rabinowitz JS, Moon RT (2014) Macrophages modulate adult zebrafish tail fin regeneration. *Dev*. doi:10.1242/dev.098459.
43. Nadeau S, Rivest S (2003) Glucocorticoids play a fundamental role in protecting the brain during innate immune response. *J Neurosci*. doi:10.1523/jneurosci.23-13-05536.2003.
44. Ariga J, Walker SL, Mumm JS (2010) Multicolor time-lapse imaging of transgenic zebrafish: visualizing retinal stem cells activated by targeted neuronal cell ablation. *J Vis Exp* (43):2–7.
45. Pagan AJ, et al. (2015) Myeloid growth factors promote resistance to mycobacterial infection by curtailing granuloma necrosis through macrophage replenishment. *Cell Host Microbe*. doi:10.1016/j.chom.2015.06.008.
46. Yamasaki R, et al. (2014) Differential roles of microglia and monocytes in the inflamed central nervous system. *J Exp Med*. doi:10.1084/jem.20132477.

47. Turk BR, et al. (2018) Dendrimer–N-acetyl-L-cysteine modulates monophagocytic response in adrenoleukodystrophy. *Ann Neurol*. doi:10.1002/ana.25303.
48. Mishra MK, et al. (2014) Dendrimer Brain Uptake and Targeted Therapy for Brain Injury in a Large Animal Model of Hypothermic Circulatory Arrest. *ACS Nano*. doi:10.1021/nn404872e.
49. White DT, Mumm JS (2013) The nitroreductase system of inducible targeted ablation facilitates cell-specific regenerative studies in zebrafish. *Methods* 62(3):232–240.
50. Mumm JS, et al. (2006) In vivo imaging reveals dendritic targeting of laminated afferents by zebrafish retinal ganglion cells. *Neuron* 52(4):609–21.
51. Ariga J, Walker SL, Mumm JS (2010) Multicolor time-lapse imaging of transgenic zebrafish: Visualizing retinal stem cells activated by targeted neuronal cell ablation. *J Vis Exp*. doi:10.3791/2093.
52. White DT, et al. (2016) ARQiv-HTS, a versatile whole-organism screening platform enabling in vivo drug discovery at high-throughput rates. *Nat Protoc* 11(12):2432–2453.

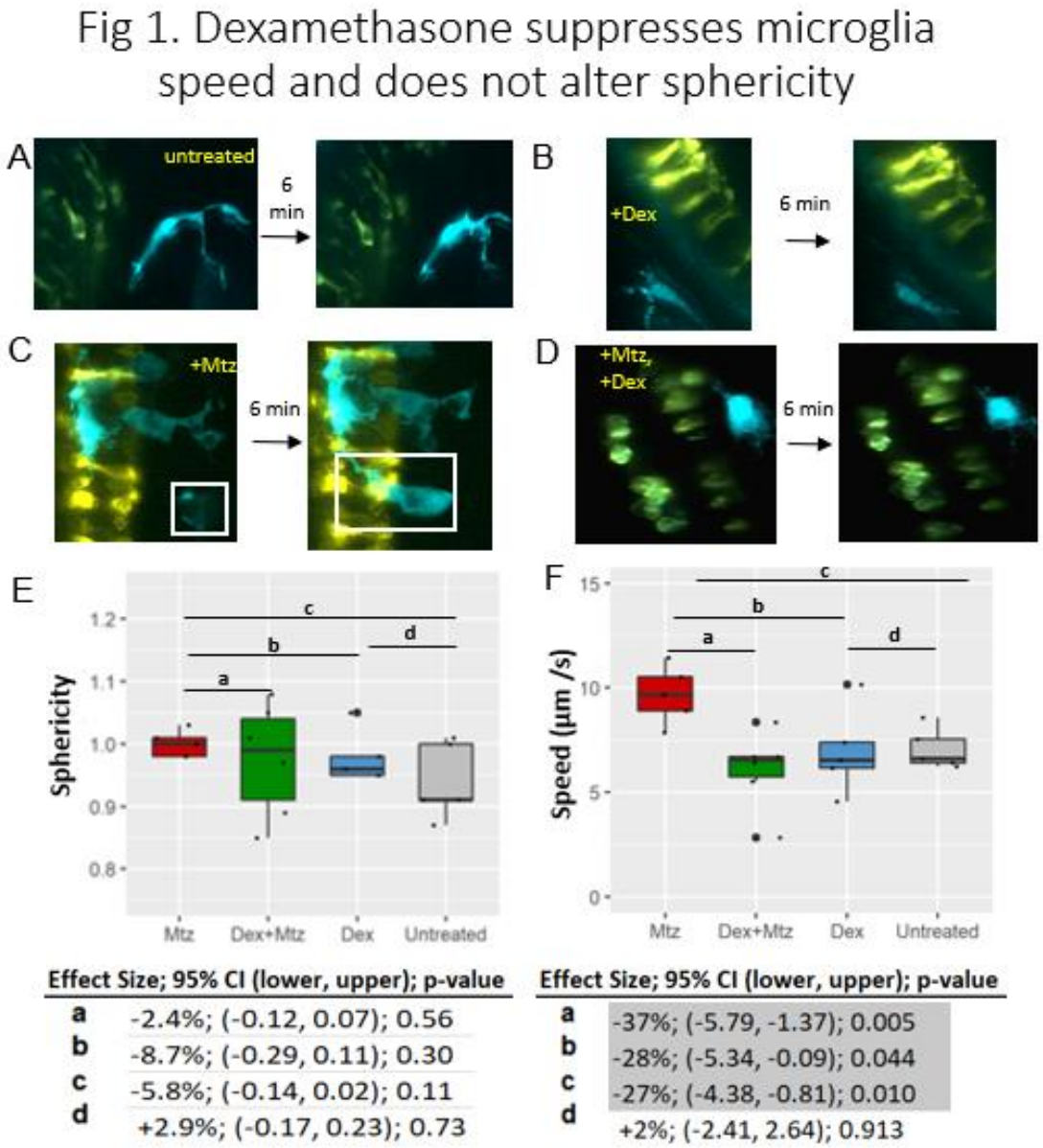

	Effect Size; 95% CI (lower, upper); p-value
a	-2.4%; (-0.12, 0.07); 0.56
b	-8.7%; (-0.29, 0.11); 0.30
c	-5.8%; (-0.14, 0.02); 0.11
d	+2.9%; (-0.17, 0.23); 0.73

	Effect Size; 95% CI (lower, upper); p-value
a	-37%; (-5.79, -1.37); 0.005
b	-28%; (-5.34, -0.09); 0.044
c	-27%; (-4.38, -0.81); 0.010
d	+2%; (-2.41, 2.64); 0.913

Figure 1. Dexamethasone suppresses microglia speed and does not alter sphericity. A-D, rod PRs (yellow) were ablated with MTZ in fish co-labeled for microglia (cyan) and a subset were treated with Dex. Fish were imaged at 5 dpf using AO-LLSM. **A-B,** Microglia in untreated fish and fish that received Dex only were ramified and often extended and contracted processes but exhibited little to no migration over time. **C,** Microglia in fish whose rod PR were ablated with MTZ (10 mM, 12 or 24 hours) migrated rapidly directly to the dying rod PRs visible over short time frames. **D,** Fish soaked with Dex post-MTZ (2.5 µM, 6 or 24 hours) exhibited comparably static microglia that did not migrate noticeably to rod PRs. **E-F,** Imaris was used to quantify sphericity and speed (µm/second) of microglia in our 4 groups (6-8 fish per condition). Statistical comparisons between groups (a-d) were done to calculate effect size, 95% confidence intervals, and p-value. See supplemental videos 1-4.

Fig 2. D-Dex injection has reduced toxicity in larval zebrafish

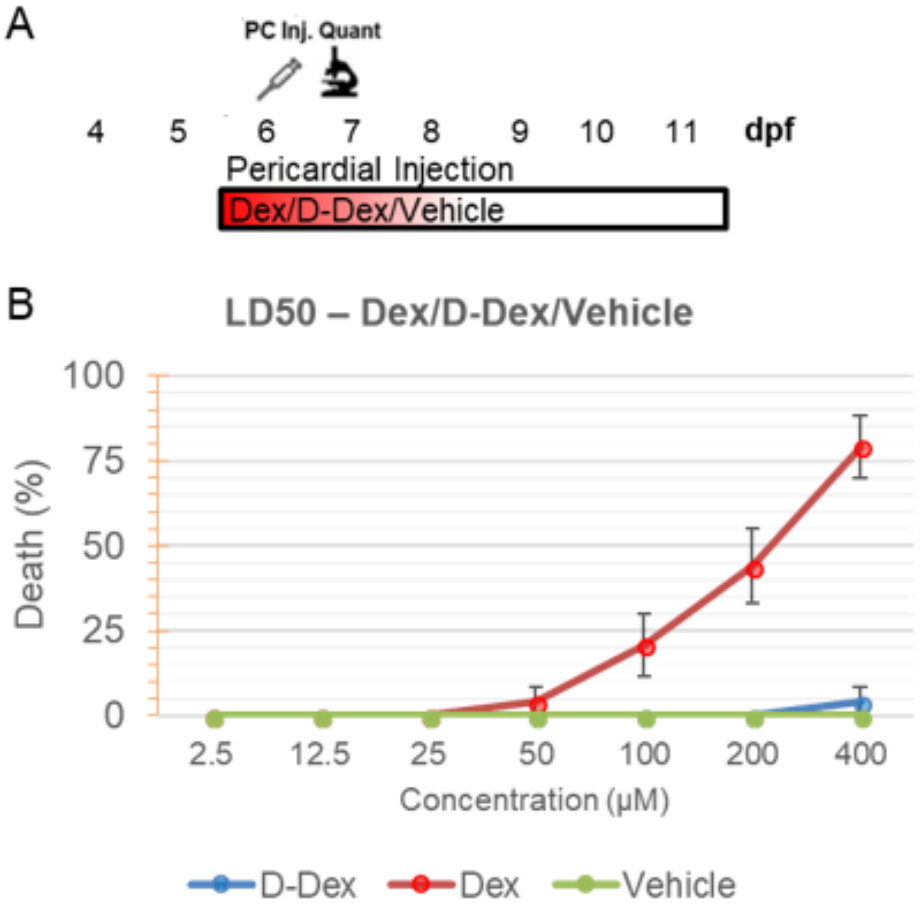

Figure 2. D-Dex injection has reduced toxicity in larval zebrafish. A, To test the relative toxicity of D-Dex, Free-Dex, and control vehicle, pericardial injections (PI) were conducted with 5 dpf zebrafish larvae (≤10nL injected volume, 2.5-400 µM for D-Dex or Free-Dex). At 7 dpf, toxicity was quantified based on percent survival. **B,** PI Dex injections displayed greatest toxicity (LD50 range between 200-400 µM). Vehicle and D-Dex had zero toxicity ≤200µM, D-Dex had minimal toxicity at 400 µM (B).

Fig 3. D-Dex treatment following Mtz ablation enhances regeneration more than free Dex

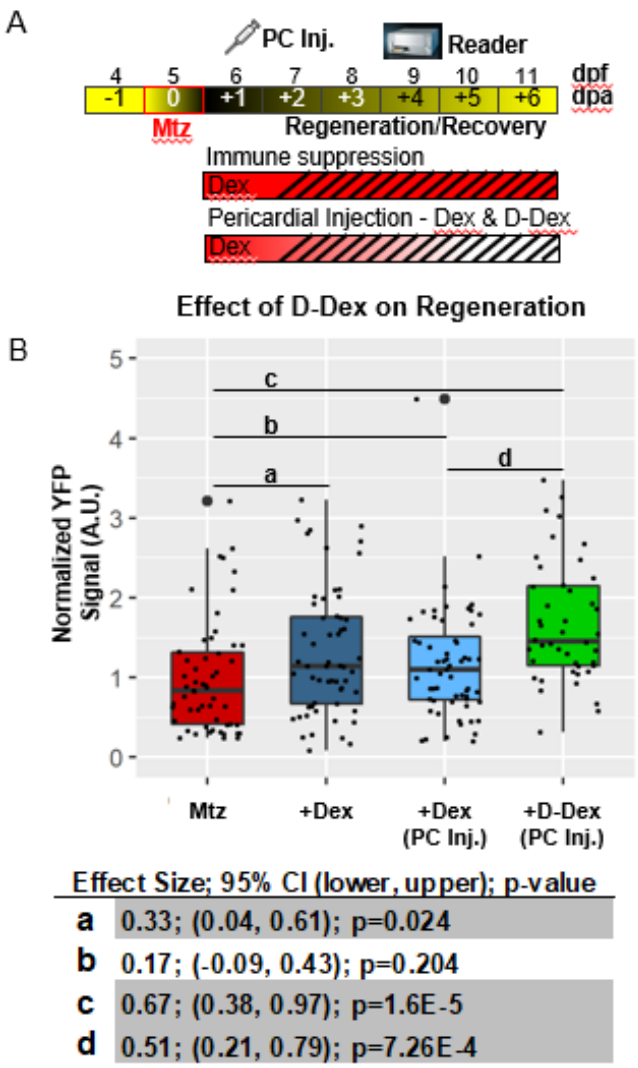

	Effect Size; 95% CI (lower, upper); p-value
a	0.33; (0.04, 0.61); p=0.024
b	0.17; (-0.09, 0.43); p=0.204
c	0.67; (0.38, 0.97); p=1.6E-5
d	0.51; (0.21, 0.79); p=7.26E-4

Figure 3. D-Dex treatment following Mtz ablation enhances regeneration more than free Dex. A, To assess regeneration kinetics, rod PRs were ablated with MTZ (5 dpf, 10 mM, 24 hours) and then treated with 2.5 µM Free-Dex or PI injection of 5 µM Free-Dex or D-Dex at 6 dpf. Three days later (9 dpf), all fish were examined with the TECAN plate reader. **B,** YFP signals across groups (MTZ only control, +Free-Dex, +PI Dex, +PI D-Dex) are plotted. Statistical comparisons between groups (a-d) were done to calculate effect size, 95% confidence intervals, and p-value.

Fig 4. Dendrimer-Cy5 localizes to dying Rod Photoreceptors

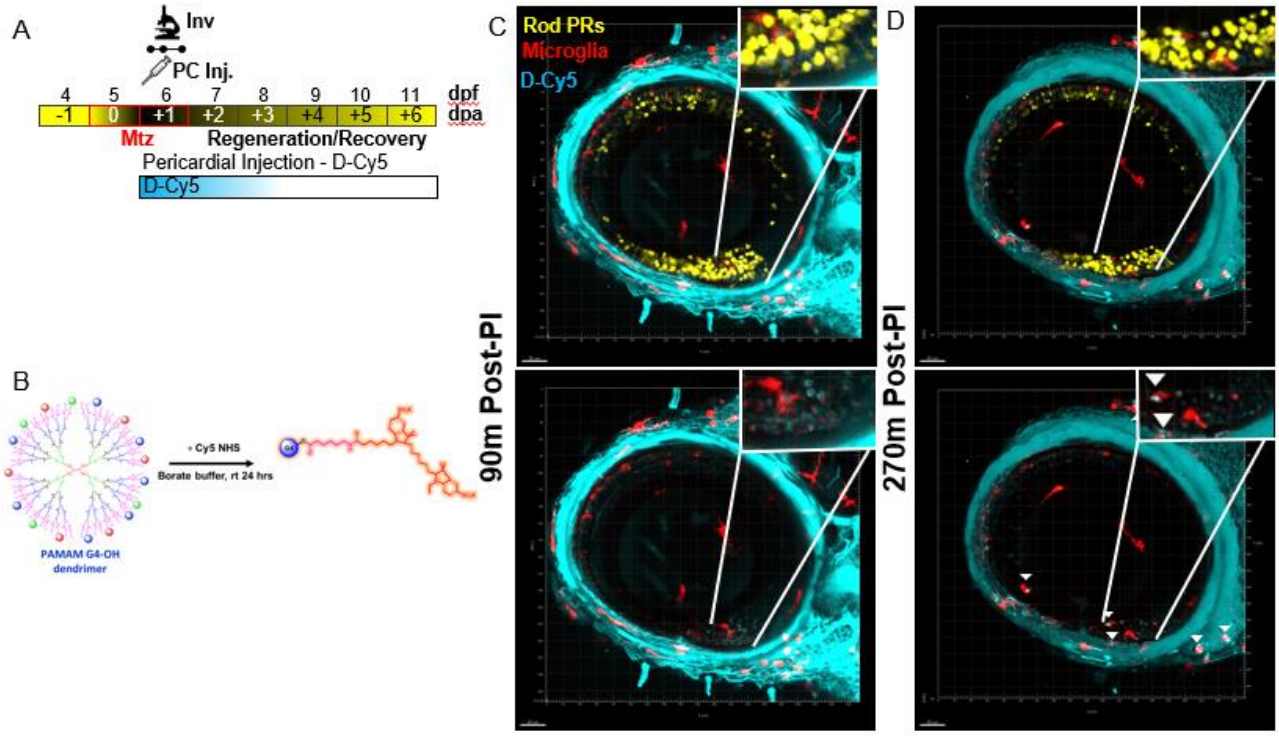

Figure 4. Dendrimer-Cy5 localizes to dying Rod Photoreceptors. A, To investigate the MoA of Dendrimer nanoparticles, fish treated with D-Cy5 following MTZ ablation were imaged. rod PRs were ablated with MTZ (5 dpf, 2.5 mM, 48 hours). At 6 dpf, fish were injected with D-Cy5 (2 ng/ul) and then imaged at differing timepoints using *in vivo* confocal microscopy. **B,** Creation of labeled D-Cy5 using PAMAM G4-OH, Cy5 NHS, and borate buffer. **C,** At 90 minutes post injection, D-Cy5 appears localized to dying rod PRs in the outer nuclear layer (ONL), YFP channel is removed for clarity in bottom image. **D,** By 270 minutes, co-labeled microglia (RFP+) that have responded to dying rod PRs appear to take up D-Cy5 in several instances, indicated by arrows in bottom image with YFP removed. See supplemental video 5.

Supp Fig 1. Morphometric analysis of D-Cy5 injected zebrafish

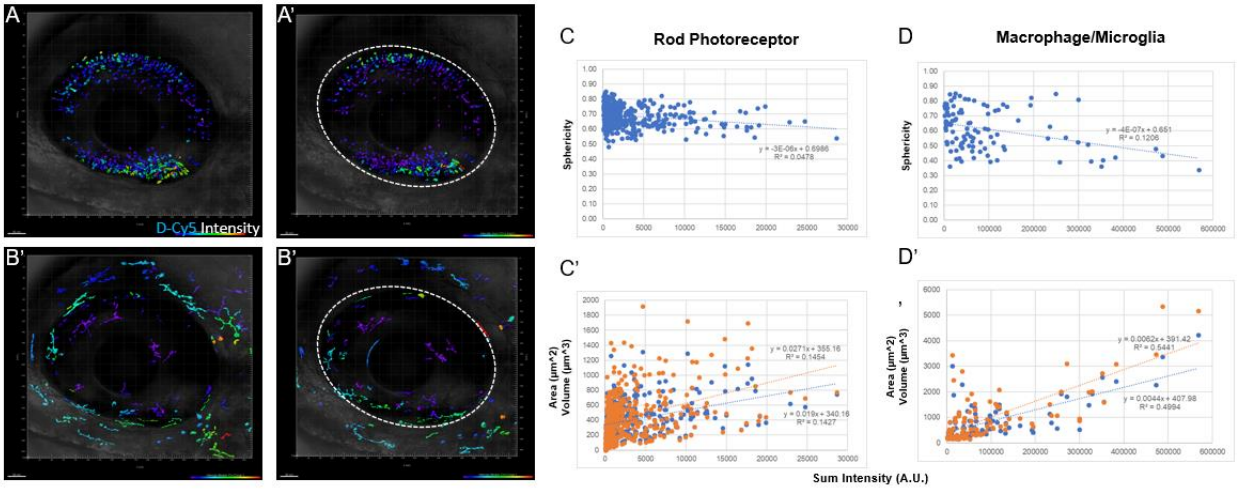

Supplemental Figure 1. Morphometric analysis of D-Cy5 injected zebrafish. A-A', To further investigate selective targeting of D-Cy5 to activated microglia, images post-D-Cy5 injections were colorized with respect to D-Cy5 fluorescent intensity. By 90 minutes, multiple sections of rod PRs are localized near injected D-Cy5 (A); the signal is somewhat diminished by 270 minutes (A'). **B-B',** Microglia near dying rod PRs at the ONL acquire D-Cy5 the fastest and generally maintain that pattern through 270 minutes. **C-C',** Morphometric analysis applied to rod PRs based on sphericity, surface area, and volume gave no observable correlation. **D-D',** Similar analyses for labeled macrophage/microglia also do not show statistical correlation as well.

Supp Fig 2. Peripheral macrophage translocation into the retina

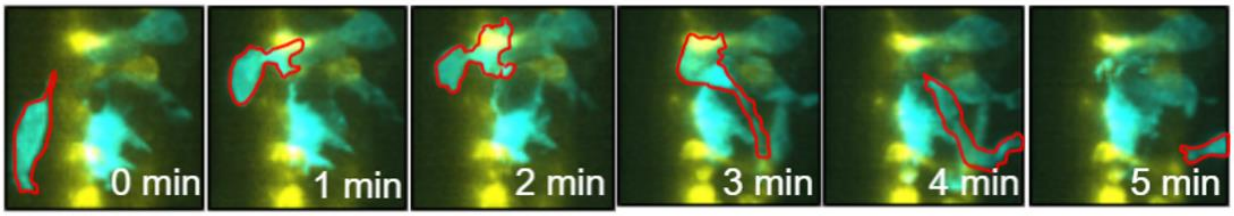

Supplemental Figure 2. Peripheral macrophage translocation into the retina. Time-lapse imaging using AO-LLSM over a five-minute time period (left to right) of rod PRs (yellow) ablated with MTZ in a fish co-labeled for microglia (cyan). Shows translocation of peripheral macrophage (outlined in red) translocating from outside of the retina to inside the retina. See supplemental video 6.